

Carbon-stabilized porous silicon as novel voltammetric sensor platforms

Clara Pérez-Ràfols^{1,8}, Keying Guo^{2,3,8}, Maria Alba^{2,3,4}, Rou Jun Toh⁴, Núria Serrano^{1,5},
Nicolas H. Voelcker^{2,3,4}, and Beatriz Prieto-Simón^{2,6,7*}

¹ Department of Chemical Engineering and Analytical Chemistry, Universitat de Barcelona, Martí i Franquès 1-11, E-08028 Barcelona (Spain)

² Disposition and Dynamics, Monash Institute of Pharmaceutical Sciences, Monash University, Parkville, 3052 Victoria (Australia)

³ Melbourne Centre for Nanofabrication, Victorian Node of the Australian National Fabrication Facility, Clayton, 3168 Victoria (Australia)

⁴ Commonwealth Scientific and Industrial Research Organisation (CSIRO) Clayton, Victoria 3168 (Australia)

⁵ Water Research Institute (IdRA) of the University of Barcelona (Spain)

⁶ Department of Electronic Engineering, Universitat Rovira i Virgili, 43007 Tarragona (Spain)

⁷ ICREA, Pg. Lluís Companys 23, Barcelona (Spain)

⁸ C. Pérez-Ràfols, K. Guo contributed equally in this study.

*Correspondence: beatriz.prieto-simon@urv.cat

ABSTRACT

The use of carbon-stabilized porous silicon (pSi) as a voltammetric sensing platform able to discriminate the detection of various electroactive species with similar redox potentials is demonstrated for the first time. For this purpose, the voltammetric responses to the presence of the three dihydroxybenzene isomers hydroquinone, catechol and resorcinol were studied using thermally hydrocarbonized pSi (THCpSi) and thermally carbonized

1 pSi (TCpSi), as well as a glassy carbon electrode (GCE) as a benchmark. Both THCpSi
2 and TCpSi outperformed the electrochemical performance of a GCE, as shown by the
3 electrochemical characterization performed in the presence of the redox pair $[\text{Fe}(\text{CN})_6]^{3-}$
4
5
6
7 ⁴⁻. Cyclic voltammetry results demonstrated that both THCpSi and TCpSi exhibited fast
8
9 electron transfer kinetics, with TCpSi showing a slightly improved electrochemical
10
11 performance. The electrode catalytic enhancement shown by these carbon-stabilized
12
13 nanostructures was harnessed to allow the simultaneous voltammetric determination of
14
15 hydroquinone, catechol and resorcinol. The analytical performance of TCpSi to the
16
17 detection of the three dihydroxybenzene isomers was studied using differential pulse
18
19 voltammetry, revealing good reproducibility, high sensitivity, low limits of detection (all
20
21 below $5 \mu\text{mol L}^{-1}$) and good recoveries (between 98% and 102%) in the analysis of spiked
22
23 tap water samples.
24
25
26
27

28
29 **Keywords:** Porous silicon; carbon stabilization; electrochemical sensor; differential
30
31 pulse voltammetry; dihydroxybenzene isomers
32
33
34
35
36
37

38 **1. INTRODUCTION**

39
40

41 Porous silicon (pSi) is a versatile porous semiconductor that has attracted attention in a
42
43 wide range of fields with applications as diverse as drug delivery, energy conversion and
44
45 sensing, among others. This wide interest is due to some of the unique features of pSi
46
47 such as its availability, biocompatibility, fast and simple fabrication process, large surface
48
49 area, adjustable pore size, thickness and porosity, and a convenient surface chemistry that
50
51 allows different routes for functionalization [1–3].
52
53
54

55
56 In particular, the possibility to control the pore morphology of pSi and its versatile surface
57
58 chemistry provide a wide range of options to design chemical sensors and biosensors. In
59
60
61
62

1 fact, pSi has been successfully applied to the development of optical and electrical
2 sensors. Optical sensors are commonly based on monitoring the shift in the
3 interferometric reflectance fringe pattern caused by changes in the average refractive
4 index [4], whereas electrical sensors usually rely on measuring either conductance or
5 capacitance changes [4]. However, little research has been done on the development of
6 electrochemical sensors based on pSi, which present some interesting features including
7 high sensitivity, low cost, relatively simple instrumentation, easy miniaturization and
8 portability [5,6]. To the best of our knowledge, the coupling of pSi with electrochemical
9 sensing has mainly been studied in the form of amperometric and impedimetric
10 biosensors [7], without further exploring the possibilities of non-functionalized
11 voltammetric pSi sensors.
12
13
14
15
16
17
18
19
20
21
22
23
24
25
26

27 While pSi presents as a promising electrochemical transducer, one of the main challenges
28 faced is the low chemical stability of freshly etched pSi. Highly reactive silicon hydride
29 species present can easily be oxidized in both water and air resulting in the formation of
30 an insulating SiO₂ layer. Stabilization methods based on pSi oxidation through thermal,
31 chemical or anodic oxidation treatments promote the growth of the insulating SiO₂ layer
32 which limits the performance of certain electrochemical transduction techniques. Other
33 approaches that have been explored to both stabilize and modify the electrical properties
34 of pSi, making it more fit for electrochemical sensing, include various thin film coating
35 methods based on metals or conductive polymers [4].
36
37
38
39
40
41
42
43
44
45
46
47
48

49 Another method that allows the stabilization of pSi is based on the introduction all over
50 its contour of an ultrathin, conformal carbon layer by thermal decomposition of acetylene.
51 This method was first introduced by Salonen *et al.* [5] and has already found many
52 applications in the fields of drug delivery, optical sensors, batteries and electrochemical
53 supercapacitors [6,8]. However, it was only recently that this stabilization method was
54
55
56
57
58
59
60
61
62
63
64
65

1 explored for the development of electrochemical sensors. Guo *et al.* [9] studied the
2 electrochemical performance of thermally hydrocarbonized pSi (THCpSi) and thermally
3 carbonized pSi (TCpSi) and demonstrated that carbon-stabilized pSi presents fast electron
4 transfer kinetics while maintaining the unique features of pSi (large surface area,
5 adjustable pore morphology, versatile surface chemistry...), rendering it suitable as
6 electrochemical platform. The development of an impedimetric immunosensor for the
7 detection of MS2 bacteriophage based on an anti-MS2 antibody-modified THCpSi
8 platform was reported, highlighting the potential of carbon-stabilized pSi for biosensing
9 applications.
10
11
12
13
14
15
16
17
18
19
20
21

22 Carbon-stabilized pSi presents some interesting features derived from the ultrathin carbon
23 layer formed during the thermal decomposition of acetylene that can be exploited to
24 widen its application to voltammetric chemical sensors with unique advantages. It has
25 been shown that the coupling of carbon-based nanomaterials with electrochemical sensors
26 not only increases their sensitivity but can also provide a better selectivity towards some
27 analytes [10,11]. Carbon-stabilized pSi is not just appealing to biosensing applications; it
28 can also be a good electrochemical platform as a bare substrate, without the need of
29 further modification, therefore constituting a clear advantage over other carbon-based
30 nanomaterials sensors.
31
32
33
34
35
36
37
38
39
40
41
42
43
44

45 Thus, in this work we report for the first time the application of non-functionalized
46 carbon-stabilized pSi in electrochemical sensing. For this purpose, the electrochemical
47 performance of both THCpSi and TCpSi was investigated via differential pulse
48 voltammetry (DPV) measurements to determine three dihydroxybenzene isomers,
49 namely catechol (CC), hydroquinone (HQ) and resorcinol (RC), commonly used as
50 chemicals in several products (e.g., cosmetics, dyes, pesticides, medicines) and
51 considered to be environmental pollutants due to their high toxicity and low degradability
52
53
54
55
56
57
58
59
60
61
62
63
64
65

1 [12,13]. The presence of CC, HQ and RC has been reported in effluents from various
2 industries (e.g. textile, pharmaceutical, plastic) and in the wastewater of synthetic coal
3 fuel conversion processes with concentrations ranging from 9 $\mu\text{mol L}^{-1}$ to 9 mmol L^{-1}
4 [14]. The direct simultaneous voltammetric determination of these three isomers is
5 usually problematic due to the close oxidation potential of HQ and CC. To tackle this
6 difficult problem without resorting to sample treatment, two main approaches can be
7 followed: (i) signal deconvolution by means of chemometric treatments or (ii)
8 improvement of the working electrode catalytic response through its modification.
9 Regarding the former approach, there have been some attempts allowing the voltammetric
10 determination of such compounds using various chemometric strategies [15–17]. In the
11 latter approach, the incorporation of several nanomaterials has been reported to enlarge
12 the separation of HQ and CC voltammetric peaks. In particular, good results have been
13 achieved by modifying the working electrode with graphene [16,18,19], carbon
14 nanotubes [11,20,21], mesoporous materials [22,23] and their combination with metal
15 nanoparticles [24–26], among others. In this work, catalytic enhancement is achieved
16 through the ultrathin carbon layer generated during carbon-stabilization of pSi, allowing
17 a good discrimination among HQ, CC and RC.
18
19
20
21
22
23
24
25
26
27
28
29
30
31
32
33
34
35
36
37
38
39
40
41
42
43
44

45 **2. MATERIALS AND METHODS**

46 **2.1. Materials**

47
48
49 6-inch, boron doped (p-type) Si wafers with 0.00055-0.001 $\Omega\text{ cm}$ resistivity, (100)-
50 oriented were purchased from Siltronix (France). Hydrofluoric acid (HF, 48%, AR grade)
51 was purchased from Scharlau (Australia). The acetylene gas cylinder (industrial grade,
52 dissolved) was purchased from BOC (Australia). Potassium ferricyanide $\text{K}_3[\text{Fe}(\text{CN})_6]$,
53
54
55
56
57
58
59
60
61
62
63
64
65

1 potassium ferrocyanide $K_4[Fe(CN)_6]$, HQ, CC, RC and phosphate buffered saline (PBS)
2 tablets were provided by Sigma-Aldrich (Australia).
3
4

5 **2.2. Instrumentation**

6
7 Scanning electron microscopy (SEM) images were obtained with a FEI NovaNano SEM
8 430 at an accelerating voltage of 10 kV. Attenuated total reflectance Fourier transform
9 infrared (ATR-FTIR) spectroscopy was performed with a Thermo Scientific Nicolet 6700
10 FTIR spectrometer. Raman spectra were acquired using a Renishaw inVia Raman
11 microscope with a 100 mW 532 nm laser excitation source. A 10% excitation power
12 density was applied to avoid damage of the surface.
13
14

15 Electrochemical measurements were performed on a CH Instrument model 600D Series
16 (CH Instruments, USA) controlled with the provided software package. A homemade
17 three-electrode Teflon cell placed in a Faraday cage, and containing the THcPsi or TCpSi
18 substrate as the working electrode, was used. The working electrode area was delimited
19 to 7.5 mm diameter by an O-ring. A Ag/AgCl/NaCl (3 mol L^{-1}) electrode provided by
20 BAS Inc (West Lafayette, IN, USA) and a platinum wire were used as reference and
21 counter electrodes, respectively. Glassy carbon electrodes (GCE) with 3 mm diameter
22 used for comparison purposes were provided by CH Instruments. All the potentials are
23 referred to Ag/AgCl.
24
25
26
27
28
29
30
31
32
33
34
35
36
37
38
39
40
41
42
43
44

45 **2.3. Fabrication of THcPsi and TCpSi**

46 **2.3.1. Fabrication of pSi**

47
48 A 6-inch Si wafer was anodically etched in an electrolyte solution containing 1:1 (v:v)
49 HF/ethanol to produce pSi, using a MPSB wet etching system (A.M.M.T GmbH,
50 Germany), which exposes an etching area of 132 cm^2 . A sacrificial layer produced with
51 a current density of 61 mA cm^{-2} for 30 s was removed with 1 mol L^{-1} sodium hydroxide
52
53
54
55
56
57
58
59
60
61
62
63
64
65

1 [27]. Then the etching cell was rinsed with water, absolute ethanol and dried with N₂ gas.
2 Next, a current density of 53 mA cm⁻² was applied to the etching cell for either 20 s or 60
3 s to form a porous film with pores of 72 ± 15 nm in diameter and a thickness of 500 nm
4 or 1.5 μm, respectively. The freshly etched pSi was finally rinsed with ethanol and dried
5 with N₂ gas to immediately proceed with its carbon stabilization. The thin film of pSi was
6 used for sensing purposes, while the thick layer of pSi was used to perform FTIR and
7 Raman measurements.
8
9
10
11
12
13
14
15
16
17
18
19

20 ***2.3.2. Carbon stabilization of pSi by thermal decomposition of acetylene gas***

21 Thermal hydrocarbonization of freshly etched pSi (THCpSi) was carried out at 525 °C
22 under a 1:1 N₂:acetylene mixture flow, whereas thermal carbonization of freshly etched
23 pSi (TCpSi) consisted on a two-step carbonization process, where THC treatment was
24 followed by annealing at 800 °C. More detailed experimental information can be found
25 elsewhere [9].
26
27
28
29
30
31
32
33
34
35

36 **2.4. Measurement of interferometric reflectance spectra**

37 Interferometric reflectance Fourier Transform spectroscopy was used to study the
38 stability of pSi, THCpSi and TCpSi. Interferometric reflectance spectra were obtained
39 using a tungsten lamp (Ocean Optics) and a CCD spectrometer (Ocean Optics S- 2000).
40 Incident light was fed through one end of a bifurcated fiber optic cable and focused
41 through a lens onto the porous films. Reflected light from the porous film was collected
42 through the same optical lens and transferred to the CCD spectrometer via the second arm
43 of the bifurcated optic cable. For reflectance measurements, the spectra were referenced
44 to a silver mirror. Reflectivity spectra were recorded in the wavelength range 350–1100
45 nm, with a spectral acquisition time of 20 ms. Igor program library was applied to the
46
47
48
49
50
51
52
53
54
55
56
57
58
59
60
61
62
63
64
65

1
2
3
4
5
6
7
8
9
10
11
12
13
14
15
16
17
18
19
20
21
22
23
24
25
26
27
28
29
30
31
32
33
34
35
36
37
38
39
40
41
42
43
44
45
46
47
48
49
50
51
52
53
54
55
56
57
58
59
60
61
62
63
64
65

resulting spectra to provide a single peak which position corresponds to the effective optical thickness (EOT). EOT monitoring provided information about the stability of the various pSi samples tested.

2.5. Electrochemical measurements

Electrochemical characterization was performed by cyclic voltammetry (CV) using 2 mmol L⁻¹ [Fe(CN)₆]^{3-/4-} in 10 mmol L⁻¹ PBS buffer (pH 7.4) as redox probe. CV measurements were performed from -0.2 to 0.8 V at a scan rate of 100 mV s⁻¹.

To assess the analytical performance of the various pSi substrates towards the electrochemical detection of the three dihydroxybenzene isomers, CC, HQ and RC, solutions of each one of those compounds were prepared daily in deaerated 10 mmol L⁻¹ PBS buffer (pH 7.4) and kept in the dark to prevent oxidation. CV measurements were performed between -0.3 and 1 V at a scan rate of 50 mV s⁻¹ and DPV measurements were performed after 30 s stirring by scanning the potential from -0.2 to 0.9 V using step potentials of 5 mV, pulse amplitudes of 50 mV and pulse times of 50 ms.

Tap water samples were collected in December 2019 from the local distribution network in Barcelona, managed by Agbar Company and mostly using water coming from Llobregat River. The collected samples were spiked with HQ and CC to a final concentration of 5.8 μmol L⁻¹ of each isomer, and pH was adjusted to 7.4 (dilution ratio 2:1). DPV measurements were carried out using the above-mentioned conditions without any further sample treatment. In addition, non-spiked tap water was scanned to confirm the absence of the target analytes.

3. RESULTS AND DISCUSSION

3.1. THCPsi and TCPsi fabrication and characterization

1 Carbon stabilization by thermal treatment of pSi in the presence of acetylene was used to
2 stabilize pSi samples. As it was previously reported by Guo *et al.* [9], this procedure
3
4 allows stabilizing pSi without altering its nanostructured morphology, which can be
5
6 controlled by adjusting the anodization conditions. Both THCpSi and TCpSi retain the
7
8 morphological features of as-prepared pSi. **Figure 1** shows the SEM images obtained for
9
10
11
12
13
14
15
16
17
18
19
20
21
22
23
24
25
26
27
28
29
30
31
32
33
34
35
36
37
38
39
40
41
42
43
44
45
46
47
48
49
50
51
52
53
54
55
56
57
58
59
60
61
62
63
64
65

FTIR and Raman spectroscopy were used to characterize the chemical composition of
freshly etched pSi, THCpSi and TCpSi. As shown by the FTIR spectra in **Figure 2a**, after
both thermal treatments, the characteristic bands of freshly etched pSi at 2087, 2114 and
905 cm^{-1} , corresponding to the stretching vibrations of Si-H and Si-H₂ and the Si-H
deformation mode, respectively, completely disappeared and were substituted by new
bands associated to saturated C-H at 2920 and 3047 cm^{-1} , unsaturated C=C stretching
vibrations at 1592 cm^{-1} , and the CH₃ symmetric deformation mode of Si-CH₃ at 1270
 cm^{-1} . Raman spectroscopy was used to confirm the successful carbonization of pSi,
shown in **Figure 2b** by the peaks depicted for both THCpSi and TCpSi at 1350 (D band)
and 1580 cm^{-1} (G band), which are Raman signatures for carbon materials [28].
Furthermore, both THCpSi and TCpSi preserved the crystallinity of Si after carbon-
stabilization, as shown by the Si lattice mode at 515 cm^{-1} .

The chemical stability of pSi, THCpSi and TCpSi was investigated by recording the
interferometric reflectance spectra obtained after exposure to 10 mM PBS buffer at pH
7.4. Both THCpSi and TCpSi single layers retain the Fabry-Pérot fringe pattern
characteristic of pSi, although with a lower intensity. The fringe maximum follows the
Fabry-Pérot relationship [27]:

$$m\lambda = 2nL \quad (1)$$

where m is an integer corresponding to the spectral order of the fringe, λ is the wavelength of incident light, n is the average refractive index of the porous matrix, and L is the physical thickness of the porous layer. The EOT referring to the $2nL$ is determined from the Fourier transform of the reflectance spectrum (**Figure 3a**). The pSi, THCpSi and TCpSi samples were incubated in PBS buffer for 15, 30, 45, 60, 105 and 180 min, washed with milliQ water and dried, before the optical spectra were recorded. The relative percentage change in EOT ($\Delta EOT\%$) was calculated as previously reported [29]:

$$\Delta EOT\% = (nL - nL_0) / nL_0 \times 100 \quad (2)$$

where nL_0 is the value measured just before exposing the sample to buffer. **Figure 3b** shows the $\Delta EOT\%$ as a function of the time exposed to PBS. The decrease in EOT observed is indicative of the degradation and subsequent dissolution of the pSi surface. While non-stabilized pSi significantly degrades over time as shown by the constant decrease in EOT after incubation in PBS, both THCpSi and TCpSi show negligible decrease in EOT ($< 1\%$) over an incubation time of 180 min. These results underpin the chemical stability of both carbon-stabilized nanostructures.

The electrochemical performance of both THCpSi and TCpSi was evaluated by CV in the presence of $2 \text{ mmol L}^{-1} [\text{Fe}(\text{CN})_6]^{3-/4-}$ in 10 mmol L^{-1} PBS buffer (pH 7.4) as redox probe. **Figure 4a** shows the CV measurements of 20 consecutive cycles for THCpSi and TCpSi samples, while **Figure 4b** shows triplicates of the nineteenth scan for both samples. The peak current and peak potential separation values extracted from the CVs in Figure 4b are summarized in **Table 1**. THCpSi and TCpSi depict well-defined $[\text{Fe}(\text{CN})_6]^{3-/4-}$ redox peaks, TCpSi showing a slightly improved electrochemical performance, inferred by the larger current intensity values and smaller peak-to-peak

1 potential difference this carbon-stabilized substrate exhibits. Both THCPsi and TCPsi
2 samples show a highly stable response along 20 consecutive measurements, with a
3 relative standard deviation (RSD) associated to the oxidation peak current of 0.5% and
4 0.2%, respectively, supporting their excellent response repeatability. The reproducibility
5 among electrodes prepared from three rounds of TC and THC treatments conducted
6 separately using the same batch of pSi samples was also outstanding, with RSD values
7 for the oxidation peak current of 0.8% and 1.8%, respectively. The slightly better
8 electrochemical performance observed for TCPsi might be attributed to its improved
9 chemical stability and higher carbon surface coverage [9].
10
11
12
13
14
15
16
17
18
19
20
21
22
23
24

25 **3.2. Electrochemical behavior of HQ, CC and RC**

26 Initially the electrochemical behavior of HQ, CC and RC prepared in PBS at pH 7.4 was
27 studied by CV using both TCPsi and THCPsi as working electrodes, and compared to
28 the behavior observed using a GCE. **Figure 5** shows the cyclic voltammograms obtained
29 for a solution containing 30 $\mu\text{mol L}^{-1}$ of either HQ, CC or RC, using each sensor.
30
31
32
33
34
35
36
37

38 As it can be seen, both HQ (**Figure 5a**) and CC (**Figure 5b**) present a similar behavior
39 using GCE, with an anodic and a cathodic peak, at 341 and -103 mV for HQ, and at 403
40 and 19 mV for CC, respectively. This corresponds to a peak potential separation (ΔE_p) of
41 444 and 384 mV for HQ and CC, respectively, which differs significantly from the 29.5
42 mV characteristic of the two-electron reactions expected in this case (**Figure 6**),
43 indicating that both HQ and CC present an irreversible electrochemical behavior at GCE.
44
45
46
47
48
49
50
51
52 On the other hand, much higher currents were achieved with both TCPsi and THCPsi,
53 which can be attributed to their larger surface area. However, in terms of reversibility
54 TCPsi showed a much better behavior, reducing the ΔE_p to 47 and 18 mV for HQ and
55 CC, respectively, which is probably due to the improved electron transfer kinetics
56
57
58
59
60
61
62
63
64
65

1 provided by the carbon-stabilized pSi. The lack of improvement in reversibility observed
2 in the case of THCPsi (ΔE_p for HQ and CC are 650 mV and 341 mV, respectively) could
3
4 be explained by its hydrophobic nature, which hinders the interaction with
5 dihydroxybenzene isomers through hydrogen bonds [30]. As previously reported by Guo
6
7 *et al.*, THCPsi features a hydrophobic surface with an estimated water contact angle
8
9 above 120°, while TCpsi presents a hydrophilic surface with a low water contact angle
10
11 of approximately 30° [9].
12
13
14
15
16

17 The electrochemical behavior of RC (**Figure 5c**) is completely different from that shown
18 by HQ and CC. No cathodic peak was observed at GCE and the anodic current was much
19 smaller than those of HQ and CC. These facts could be attributed to the low
20 thermodynamic stability of the RC quinonic form and the lack of aromatic ring activation
21 due to the OH groups at meta- position [31]. Regarding the carbon-stabilized pSi
22 substrates, the RC anodic peak was only observed in the case of TCpsi, where it was
23 shifted to less positive potentials.
24
25
26
27
28
29
30
31
32
33
34

35 Considering these results and in particular both the slightly better stability shown in the
36 CV characterization with $[\text{Fe}(\text{CN})_6]^{3-/4-}$ and the improved electron transfer kinetics that
37 gives rise to a more reversible behavior of HQ and CC, TCpsi was selected as the best
38 carbon-stabilized pSi substrate for voltammetric chemical sensing and considered for
39 further studies.
40
41
42
43
44
45
46
47

48 In this sense, its applicability to the simultaneous determination of HQ, CC and RC was
49 evaluated by DPV. **Figure 7** shows the representative voltammograms obtained for a
50 solution containing 30 $\mu\text{mol L}^{-1}$ of HQ, CC and RC in 10 mmol L^{-1} PBS buffer at pH 7.4
51 for TCpsi and GCE. In the case of GCE only RC can be correctly determined since the
52 oxidation peaks obtained for HQ and CC totally overlap, whereas in the case of TCpsi
53
54
55
56
57
58
59
60
61
62
63
64
65

1 three separate oxidation peaks corresponding to HQ, CC and RC were obtained, allowing
2 the simultaneous determination of the three isomers.
3
4

5 **3.3. Analytical performance of TCpSi**

6

7
8 The analytical performance of TCpSi for the voltammetric determination of HQ, CC and
9 RC was evaluated. First of all, some experimental parameters such as pH and the stirring
10 time applied to accumulate the compounds on the electrodic surface, were optimized. The
11 voltammetric signals are highly influenced by pH due to the two protons involved in the
12 oxidation processes, which result in a considerable shift to more negative potentials at
13 higher pH values (**Figure S1**). However, from pH 4 to 8 the discrimination between the
14 oxidation peaks of HQ and CC could not be improved because the peaks are shifted with
15 pH at an almost identical rate for the two isomers (**Figure S1d**). In terms of current, the
16 signal increased from pH 4 to 7.5 and slightly decreased at pH 8. Thus, the physiological
17 pH (7.4) was selected as the optimal pH value.
18
19
20
21
22
23
24
25
26
27
28
29
30
31

32
33 Regarding the stirring time, voltammetric measurements using TCpSi were performed
34 using a solution containing 30 $\mu\text{mol L}^{-1}$ of HQ, CC or RC in 10 mmol L^{-1} PBS buffer at
35 pH 7.4, and varying the stirring time from 0 to 240 s. For all three isomers, the current
36 slightly increased after 30 s of stirring but no further increase was observed for longer
37 stirring times. Therefore, a stirring time of 30 s was selected as the optimal value.
38
39
40
41
42
43
44

45 Once the experimental conditions were optimized, the analytical performance of the use
46 of TCpSi for the determination of HQ, CC and RC was studied considering repeatability,
47 reproducibility, sensitivity, linear range and limits of detection (LOD) and quantification
48 (LOQ). All these values are summarized in **Table 2**.
49
50
51
52
53

54
55 Repeatability was calculated from five consecutive measurements of a solution
56 containing 30 $\mu\text{mol L}^{-1}$ of HQ, CC and RC in 10 mmol L^{-1} PBS buffer at pH 7.4 using the
57 same electrode, whereas reproducibility was computed from the slope of two independent
58
59
60
61
62
63
64
65

1 and individual calibration curves carried out from 0.5 to 50 $\mu\text{mol L}^{-1}$ and using different
2 sensors. For all three isomers, repeatability and reproducibility values lower than 6.5%
3
4 were achieved. These values are similar to those reported in the literature for GCE
5
6 modified with different carbon nanomaterials like graphene [18,19], mesoporous carbon
7
8 [23] or carbon nanotubes [11,20,21], for which repeatability and reproducibility values
9
10 were in the range of 0.85 – 3.4 % and 4.1 – 6.6 %, respectively. TCpSi's improved
11
12 reproducibility, added to its advantage of acting as both support and modifier
13
14 simultaneously, offsets the slightly higher repeatability values obtained. Indeed, the
15
16 possibility to work with unmodified TCpSi fast-tracks its fabrication process,
17
18 underpinning mass-production of working electrodes which are stable for long-term
19
20 storage at room temperature.
21
22
23
24
25

26 In terms of sensitivity, calculated as the slope of the calibration curve, HQ and CC showed
27
28 similar values, which are significantly higher than that achieved for RC. This agrees with
29
30 the more intense peaks observed for HQ and CC. On the other hand, LODs and LOQs
31
32 were calculated as three and ten times, respectively, the standard deviation of the intercept
33
34 over the slope of the calibration curves. In all cases LOQs were at the level of few μmol
35
36 L^{-1} , achieving the lowest value for HQ and the highest for RC. However, it should also
37
38 be pointed out that only RC shows a linear response up to 50 $\mu\text{mol L}^{-1}$. For HQ and CC,
39
40 the response was linear up to 35.2 and 25.4 $\mu\text{mol L}^{-1}$, respectively, leading to linear ranges
41
42 comparable to those reported by a GCE modified with mesoporous carbon CMK-3 [23]
43
44 or a commercial graphene screen-printed electrode [16], but narrower than most carbon
45
46 nanotube-modified GCEs [20, 21, 24]. Although the LODs and LOQs achieved are ~~only~~
47
48 slightly higher than those reported in the literature for GCE modified with different
49
50 nanomaterials [11,18,20,21,23], they are ~~and~~ similar to those reported for a commercial
51
52 graphene screen-printed electrode [16] (**Table S1**) and below the HQ, CC and RC levels
53
54
55
56
57
58
59
60
61
62
63
64
65

1
2
3
4
5
6
7
8
9
10
11
12
13
14
15
16
17
18
19
20
21
22
23
24
25
26
27
28
29
30
31
32
33
34
35
36
37
38
39
40
41
42
43
44
45
46
47
48
49
50
51
52
53
54
55
56
57
58
59
60
61
62
63
64
65

found in industrial effluents and wastewater, with the additional advantages provided by pSi (versatility, biocompatibility, fast and simple fabrication process, adjustable morphology...). Therefore, the fast electron transfer kinetics and the good analytical performance of TCpSi highlight its potential to act as a new substrate for voltammetric sensors able to discriminate among chemical compounds with similar electroactive behavior.

3.4. Application to the analysis of real samples

The applicability of TCpSi for the voltammetric determination of dihydroxybenzene isomers in real samples was evaluated through the determination of a tap water sample spiked with HQ and CC, as the two most problematic isomers. The simultaneous determination of these two compounds was carried out in triplicate and by means of the standard addition method, considering four successive additions. Representative differential pulse voltammograms for the analysis of the spiked tap water sample using TCpSi as working electrode are shown in **Figure 8**. Well-defined and discriminated peaks that increase linearly with the concentration were obtained for both HQ and CC.

The results obtained from the three replicates of the standard addition calibration are summarized in **Table 3**. Good agreement between replicates, as well as with the expected concentration were achieved for both HQ and CC, resulting in high recoveries and low RSDs, and confirming the applicability of TCpSi to the simultaneous determination of HQ and CC in real samples.

4. CONCLUSIONS

1 The application of carbon-stabilized pSi, without any additional modifier, as
2 voltammetric sensor platform for the simultaneous detection of three dihydroxybenzene
3 isomers has been successfully demonstrated. First of all, the electrochemical performance
4 of TCpSi and THCpSi with special focus on the repeatability and reproducibility was
5 compared. Second, the electrochemical response of both TCpSi and THCpSi to HQ, CC
6 and RC, was assessed, concluding that TCpSi offers a more reproducible response with
7 faster electron transfer kinetics that results in higher redox reversibility. Interestingly,
8 TCpSi presented a better electrochemical response to HQ, CC and RC than GCE, not only
9 inferred by the higher reversibility, but also by the possibility to simultaneously determine
10 the three dihydroxybenzene isomers. Excellent analytical performance was achieved by
11 TCpSi for the detection of the three isomers, with repeatability, reproducibility and LODs
12 similar to those reported for nanomaterial-modified GCE or screen-printed electrodes.
13 Furthermore, the applicability of TCpSi in real samples was successfully verified through
14 the analysis of a tap water sample spiked with both HQ and CC, achieving high recoveries
15 and precision. Additionally, it should be highlighted that TCpSi retains the unique
16 advantages provided by pSi, such as versatility, biocompatibility, fast and simple
17 fabrication process, and adjustable morphology, which can be harnessed to develop
18 sensing tools fit-for-purpose.

46 **ACKNOWLEDGMENTS**

49 Authors acknowledge financial support from the Australian Research Council's
50 Discovery and Linkage Project Schemes (DP160104362 and LP160101050). Clara Pérez-
51 Ràfols acknowledges the Spanish Ministry of Education, Culture and Sports for a Ph.D
52 (reference FPU15/02140) and mobility (EST17/00326) grant. This work was performed

1
2
3
4
5
6
7
8
9
10
11
12
13
14
15
16
17
18
19
20
21
22
23
24
25
26
27
28
29
30
31
32
33
34
35
36
37
38
39
40
41
42
43
44
45
46
47
48
49
50
51
52
53
54
55
56
57
58
59
60
61
62
63
64
65

in part at the Melbourne Centre for Nanofabrication (MCN) in the Victorian Node of the Australian National Fabrication Facility (ANFF).

REFERENCES

- [1] L. Canham, Handbook of porous silicon, 2nd ed., Springer, Birmingham, UK, 2017. doi:10.1007/978-3-319-04508-5.
- [2] M.J. Sailor, Fundamentals of porous silicon preparation, in: Porous Silicon Pract. Prep. Charact. Appl., Wiley-VCH Verlag GmbH & Co. KGaA, Weinheim, Germany, 2012: pp. 1–42. doi:10.1002/9783527641901.
- [3] M.P. Stewart, J.M. Buriak, Chemical and biological applications of porous silicon technology, Adv. Mater. 12 (2000) 859–869. doi:10.1002/1521-4095(200006)12:12<859::AID-ADMA859>3.0.CO;2-0.
- [4] A. Salis, S. Setzu, M. Monduzzi, G. Mula, S. Chimiche, C. Csgi, D. Fisica, U. Cagliari, Porous silicon-based electrochemical biosensors, in: Biosensors-Emerging Mater. Appl., InTech, London, UK, 2011.
- [5] J. Salonen, V.-P. Lehto, M. Björkqvist, E. Laine, L. Niinistö, Studies of thermally-carbonized porous silicon surfaces, Phys. Status Solidi A. 182 (2002) 123–126. doi:10.1002/1521-396x(200011)182:1<123::aid-pssa123>3.3.co;2-6.
- [6] J. Salonen, E. Mäkilä, Thermally carbonized porous silicon and its recent applications, Adv. Mater. 30 (2018) 1703819–1703837. doi:10.1002/adma.201703819.
- [7] C. RoyChaudhuri, A review on porous silicon based electrochemical biosensors: Beyond surface area enhancement factor, Sensors Actuators, B Chem. 210 (2015) 310-323. doi: 10.1016/j.snb.2014.12.089.
- [8] J. Salonen, M. Kaasalainen, O.-P. Rauhala, L. Lassila, M. Hakamies, T. Jalkanen,

- 1
2
3
4
5
6
7
8
9
10
11
12
13
14
15
16
17
18
19
20
21
22
23
24
25
26
27
28
29
30
31
32
33
34
35
36
37
38
39
40
41
42
43
44
45
46
47
48
49
50
51
52
53
54
55
56
57
58
59
60
61
62
63
64
65
- R. Hahn, P. Schmuki, E. Mäkilä, Thermal carbonization of porous silicon: the current status and recent applications, *ECS Trans.* 69 (2015) 167–176. doi:10.1149/06902.0167ecst.
- [9] K. Guo, A. Sharma, R.J. Toh, E. Álvarez de Eulate, T.R. Gengenbach, X. Cetó, N.H. Voelcker, B. Prieto-Simón, Porous silicon nanostructures as effective faradaic electrochemical sensing platforms, *Adv. Funct. Mater.* 29 (2019) 1809206–1809217. doi:10.1002/adfm.201809206.
- [10] C. Pérez-Ràfols, N. Serrano, J.M. Díaz-cruz, C. Ariño, M. Esteban, New approaches to antimony film screen-printed electrodes using carbon-based nanomaterials substrates, *Anal. Chim. Acta.* 916 (2016) 17–23. doi:10.1016/j.aca.2016.03.003.
- [11] H. Qi, C. Zhang, Simultaneous determination of hydroquinone and catechol at a glassy carbon electrode modified with multiwall carbon nanotubes, *Electroanalysis.* 17 (2005) 832–838. doi:10.1002/elan.200403150.
- [12] EEC Directive 80/77/CEE 15-7-1990. *Off. J. Eur. Communities* (30/08/1990), European Community, Bruselles, 1990.
- [13] Límites de exposición profesional para agentes químicos en España, Instituto Nacional de Seguridad e Higiene en el Trabajo (INSHT), 2014.
- [14] S. Suresh, V.C. Srivastava, I.M. Mishra, Adsorption of catechol, resorcinol, hydroquinone, and their derivatives: a review. *Int J Energy Environ Eng* 3, (2012) 32. <https://doi.org/10.1186/2251-6832-3-32>
- [15] K. Martínez, C. Ariño, J.M. Díaz-Cruz, N. Serrano, M. Esteban, Multivariate standard addition for the analysis of overlapping voltammetric signals in the presence of matrix effects: application to the simultaneous determination of hydroquinone and catechol, *Chemom. Intell. Lab. Syst.* 178 (2018) 32–38.

doi:10.1016/j.chemolab.2018.05.002.

- 1
2
3
4
5
6
7
8
9
10
11
12
13
14
15
16
17
18
19
20
21
22
23
24
25
26
27
28
29
30
31
32
33
34
35
36
37
38
39
40
41
42
43
44
45
46
47
48
49
50
51
52
53
54
55
56
57
58
59
60
61
62
63
64
65
- [16] M. Aragón, C. Ariño, À. Dago, J.M. Díaz-Cruz, M. Esteban, Simultaneous determination of hydroquinone, catechol and resorcinol by voltammetry using graphene screen-printed electrodes and partial least squares calibration, *Talanta*. 160 (2016) 138–143. doi:10.1016/j.talanta.2016.07.007.
- [17] M.A. Tapia, C. Pérez-Ràfols, C. Ariño, N. Serrano, J.M. Díaz-Cruz, New approach to multivariate standard addition based on multivariate curve resolution by alternating least-squares: Application to voltammetric data, *Anal. Chem.* 92 (2020) 3396–3402. doi:10.1021/acs.analchem.9b05477.
- [18] H. Du, J. Ye, J. Zhang, X. Huang, C. Yu, A voltammetric sensor based on graphene-modified electrode for simultaneous determination of catechol and hydroquinone, *J. Electroanal. Chem.* 650 (2011) 209–213. doi:10.1016/j.jelechem.2010.10.002.
- [19] T. Gan, J. Sun, K. Huang, L. Song, Y. Li, A graphene oxide-mesoporous MnO₂ nanocomposite modified glassy carbon electrode as a novel and efficient voltammetric sensor for simultaneous determination of hydroquinone and catechol, *Sensors Actuators, B Chem.* 177 (2013) 412–418. doi:10.1016/j.snb.2012.11.033.
- [20] Y.P. Ding, W.L. Liu, Q.S. Wu, X.G. Wang, Direct simultaneous determination of dihydroxybenzene isomers at C-nanotube-modified electrodes by derivative voltammetry, *J. Electroanal. Chem.* 575 (2005) 275–280. doi:10.1016/j.jelechem.2004.09.020.
- [21] D.M. Zhao, X.H. Zhang, L.J. Feng, L. Jia, S.F. Wang, Simultaneous determination of hydroquinone and catechol at PASA/MWNTs composite film modified glassy carbon electrode, *Colloids Surfaces B Biointerfaces.* 74 (2009) 317–321.

doi:10.1016/j.colsurfb.2009.07.044.

- 1
2
3
4
5
6
7
8
9
10
11
12
13
14
15
16
17
18
19
20
21
22
23
24
25
26
27
28
29
30
31
32
33
34
35
36
37
38
39
40
41
42
43
44
45
46
47
48
49
50
51
52
53
54
55
56
57
58
59
60
61
62
63
64
65
- [22] M.A. Ghanem, Electrocatalytic activity and simultaneous determination of catechol and hydroquinone at mesoporous platinum electrode, *Electrochem. Commun.* 9 (2007) 2501–2506. doi:10.1016/j.elecom.2007.07.023.
- [23] J. Yu, W. Du, F. Zhao, B. Zeng, High sensitive simultaneous determination of catechol and hydroquinone at mesoporous carbon CMK-3 electrode in comparison with multi-walled carbon nanotubes and Vulcan XC-72 carbon electrodes, *Electrochim. Acta.* 54 (2009) 984–988. doi:10.1016/j.electacta.2008.08.029.
- [24] L.A. Goulart, R. Gonçalves, A.A. Correa, E.C. Pereira, L.H. Mascaro, Synergic effect of silver nanoparticles and carbon nanotubes on the simultaneous voltammetric determination of hydroquinone, catechol, bisphenol A and phenol, *Microchim. Acta.* 185 (2018). doi:10.1007/s00604-017-2540-5.
- [25] Y. Wang, Y. Xiong, J. Qu, J. Qu, S. Li, Selective sensing of hydroquinone and catechol based on multiwalled carbon nanotubes/polydopamine/gold nanoparticles composites, *Sensors Actuators, B Chem.* 223 (2016) 501–508. doi:10.1016/j.snb.2015.09.117.
- [26] J. Tashkhourian, M. Daneshi, F. Nami-Ana, M. Behbahani, A. Bagheri, Simultaneous determination of hydroquinone and catechol at gold nanoparticles mesoporous silica modified carbon paste electrode, *J. Hazard. Mater.* 318 (2016) 117–124. doi:10.1016/j.jhazmat.2016.06.049.
- [27] B. Sciacca, E. Secret, S. Pace, P. Gonzalez, F. Geobaldo, F. Quignard, F. Cunin, Chitosan-functionalized porous silicon optical transducer for the detection of carboxylic acid-containing drugs in water, *J. Mater. Chem.* 21 (2011) 2294–2302. doi:10.1039/c0jm02904a.
- [28] R. Hawaldar, P. Merino, M.R. Correia, I. Bdikin, J. Grácio, J. Méndez, J.A. Martín-

1 Gago, M.K. Singh, Large-area high-throughput synthesis of monolayer graphene
2 sheet by hot filament thermal chemical vapor deposition, *Sci. Rep.* 2 (2012) 682.
3
4 doi:10.1038/srep00682.
5
6

7 [29] C.K. Tsang, T.L. Kelly, M.J. Sailor, Y.Y. Li, Highly stable porous silicon-carbon
8 composites as label-free optical biosensors, *ACS Nano.* 6 (2012) 10546–10554.
9
10 doi:10.1021/nn304131d.
11
12

13 [30] J. Saiz-Poseu, J. Mancebo-Aracil, F. Nador, F. Busqué, D. Ruiz-Molina., The
14 chemistry behind catechol-based adhesion, *Angew. Chem. Int. Ed.* 58 (2019) 696-
15
16 714. doi: 10.1002/anie.201801063
17
18

19 [31] B. Nasr, G. Abdellatif, P. Cañizares, C. Sáez, J. Lobato, M.A. Rodrigo,
20
21 Electrochemical oxidation of hydroquinone, resorcinol, and catechol on boron-
22 doped diamond anodes, *Environ. Sci. Technol.* 39 (2005) 7234–7239.
23
24
25
26
27
28
29
30
31
32
33
34
35
36
37
38
39
40
41
42
43
44
45
46
47
48
49
50
51
52
53
54
55
56
57
58
59
60
61
62
63
64
65

Table 1. Peak current and peak potential difference ΔE_p (mV) extracted from CV using THCpSi and TCpSi as working electrodes (n=3).

| | I_{ox} (μA) | I_{red} (μA) | ΔE_p (mV) |
|--------|---|--|-------------------------------------|
| THCpSi | 328 ± 6 | 308 ± 12 | 90 ± 15 |
| TCpSi | 364 ± 3 | 351 ± 6 | 80 ± 5 |

*All these values were extracted from the nineteenth CV scan.

Table 2. Calibration parameters, reproducibility and repeatability for the separate determination of HQ, CC and RC prepared in 10 mmol L⁻¹ PBS at pH 7.4, after 30 s of stirring, obtained using TCpSi as working electrode. Standard deviations are denoted by parenthesis (n=2).

| | HQ | CC | RC |
|--|-------------|-------------|-------------|
| Sensitivity ($\mu\text{A } \mu\text{mol}^{-1} \text{L}$) | 1.41 (0.03) | 1.55 (0.08) | 0.32 (0.01) |
| R^2 | 0.992 | 0.997 | 0.990 |
| Linear range ($\mu\text{mol L}^{-1}$) ¹ | 4.6 – 35.2 | 8.0 – 25.4 | 10.4 – 50.0 |
| LOD ($\mu\text{mol L}^{-1}$) | 1.4 | 2.4 | 3.1 |
| Reproducibility (% , n=2) | 2.4 | 6.2 | 2.9 |
| Repeatability (% , n=5) | 5.1 | 3.5 | 5.8 |

¹ The lowest value of the linear range was considered from the LOQ.

Table 3. Calibration data for the simultaneous determination of HQ and CC, spiked in a tap water sample, by DPV and using TCpSi as working electrode.

| | HQ | CC |
|--|-----------|-----------|
| C_{expected} ($\mu\text{mol L}^{-1}$) | 5.84 | 5.84 |
| C_{found} ($\mu\text{mol L}^{-1}$) | 5.91 | 5.76 |
| Recovery (%) | 101.4 | 98.6 |
| RSD (% , n=3) | 5.7 | 5.8 |

Figure captions

Figure 1. (a) Top and (b) cross-sectional SEM images of TCpSi nanostructures. The pSi layer was electrochemically etched in a 1:1 (v:v) HF/ethanol solution by applying a current density of 53 mA cm^{-2} for 20 s in a MPSB wet etching system.

Figure 2. (a) FTIR and (b) Raman spectra of freshly etched pSi, THCpSi and TCpSi. The pSi layer was electrochemically etched in a 1:1 (v:v) HF/ethanol solution by applying a current density of 53 mA cm^{-2} for 60 s in a MPSB wet etching system.

Figure 3. Stability test of pSi, THCpSi and TCpSi incubated in aqueous PBS buffer (pH 7.4) based on reflective interferometric Fourier transform spectroscopy measurements. (a) Typical Fourier transform of the reflectance spectrum (inset) of a pSi single layer with a pore diameter of $12 \pm 5 \text{ nm}$ and a thickness of $1.6 \mu\text{m}$. (b) Plot of the $\Delta\text{EOT}\%$ measured in air against incubation time in PBS.

Figure 4. (a) 20 consecutive CV scans measured in a 2 mmol L^{-1} ferrocyanide/ferricyanide solution in 10 mmol L^{-1} PBS buffer at pH 7.4 using THCpSi and TCpSi; (b) nineteenth CV scans corresponding to replicates of three THCpSi and three TCpSi samples.

Figure 5. Cyclic voltammograms obtained when testing a $30 \mu\text{mol L}^{-1}$ (a) HQ, (b) CC or (c) RC solution in 10 mmol L^{-1} PBS buffer at pH 7.4, using GCE (blue line), TCpSi (red line) and THCpSi (green line). GCE currents are referred to the right axis whereas TCpSi and THCpSi currents are referred to the left axis.

Figure 6. Redox reactions of (1) HQ, (2) CC and (3) RC.

Figure 7. Differential pulse voltammograms obtained for a solution combining $30 \mu\text{mol L}^{-1}$ HQ, CC and RC in 10 mmol L^{-1} PBS at pH 7.4, using TCpSi (red lines) and GCE (blue lines) as working electrode. GCE currents are referred to the right axis, whereas TCpSi currents are referred to the left axis.

Figure 8. Differential pulse voltammograms obtained for the simultaneous determination of HQ and CC, spiked in a tap water sample, using TCpSi as working electrode at pH 7.4 following the above stated electrochemical conditions. Inset: standard addition plots.

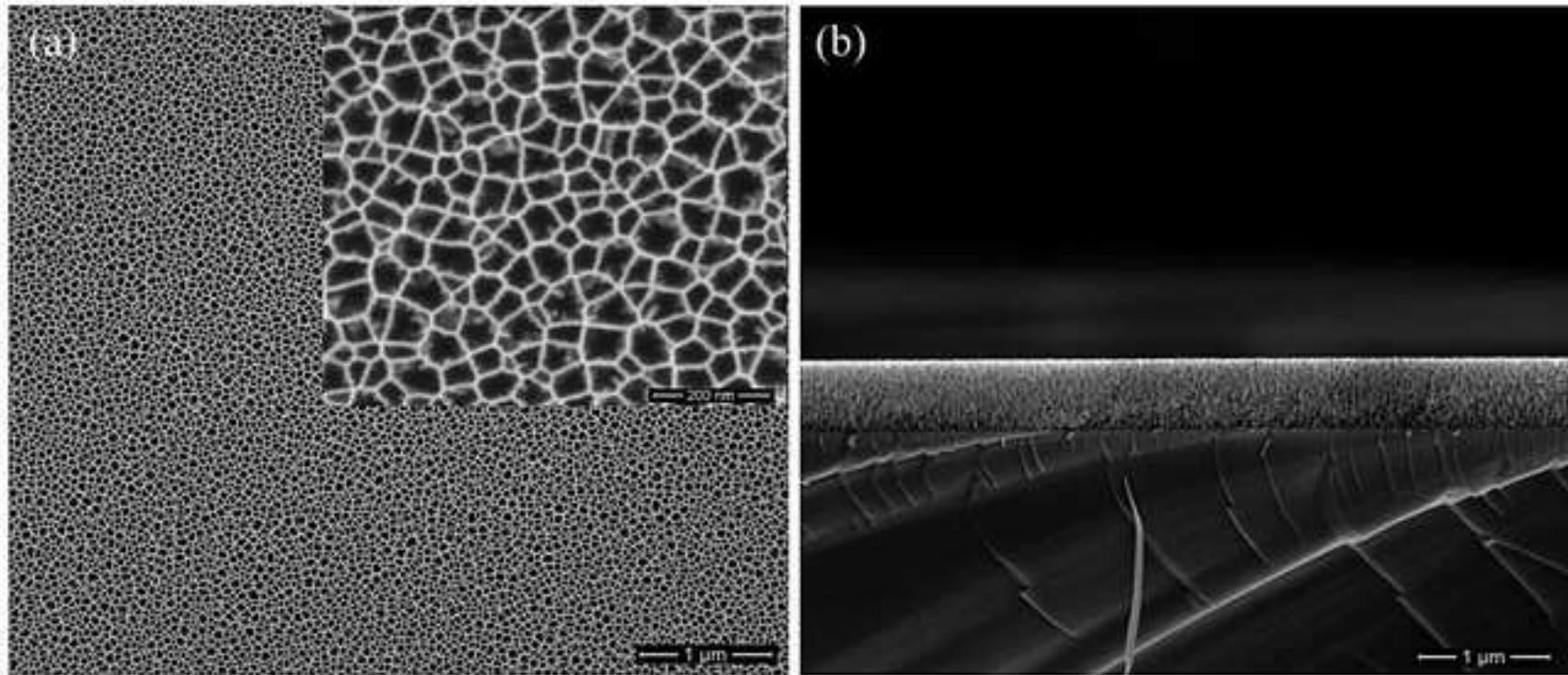
Figure 1

Figure 2

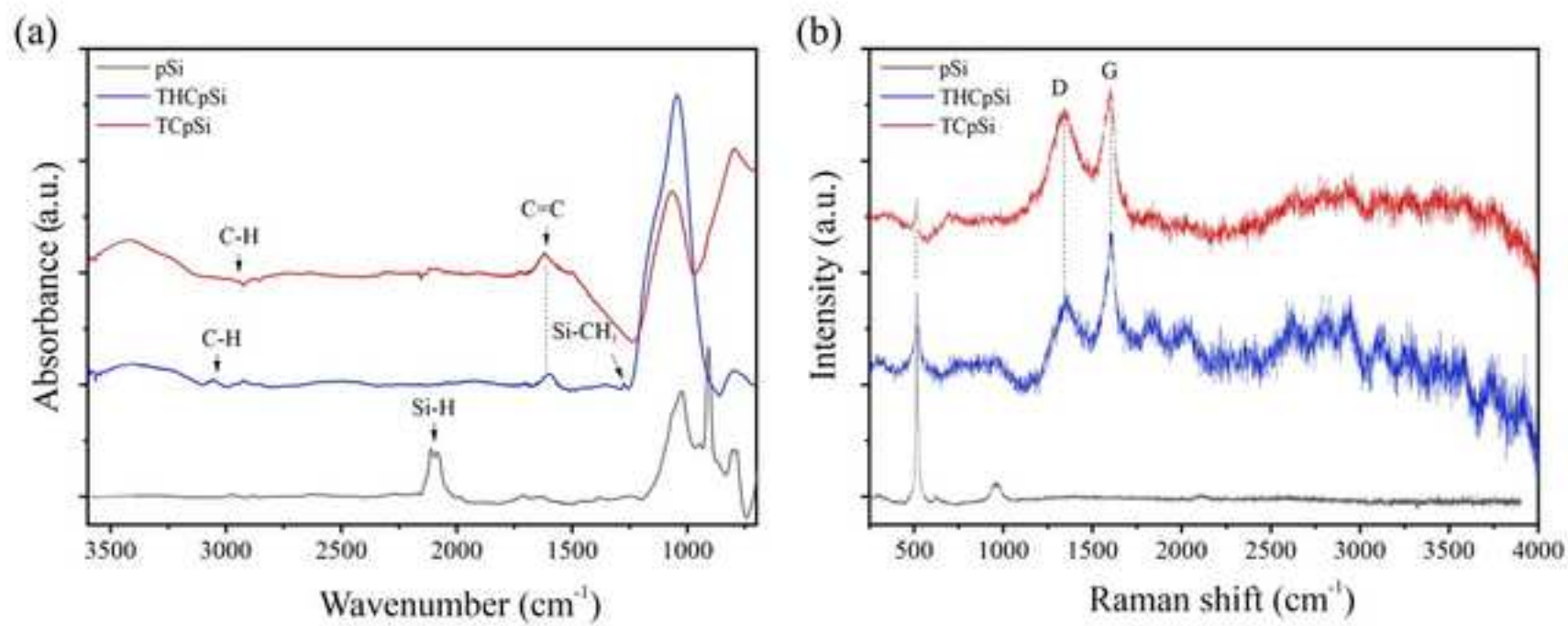


Figure 3

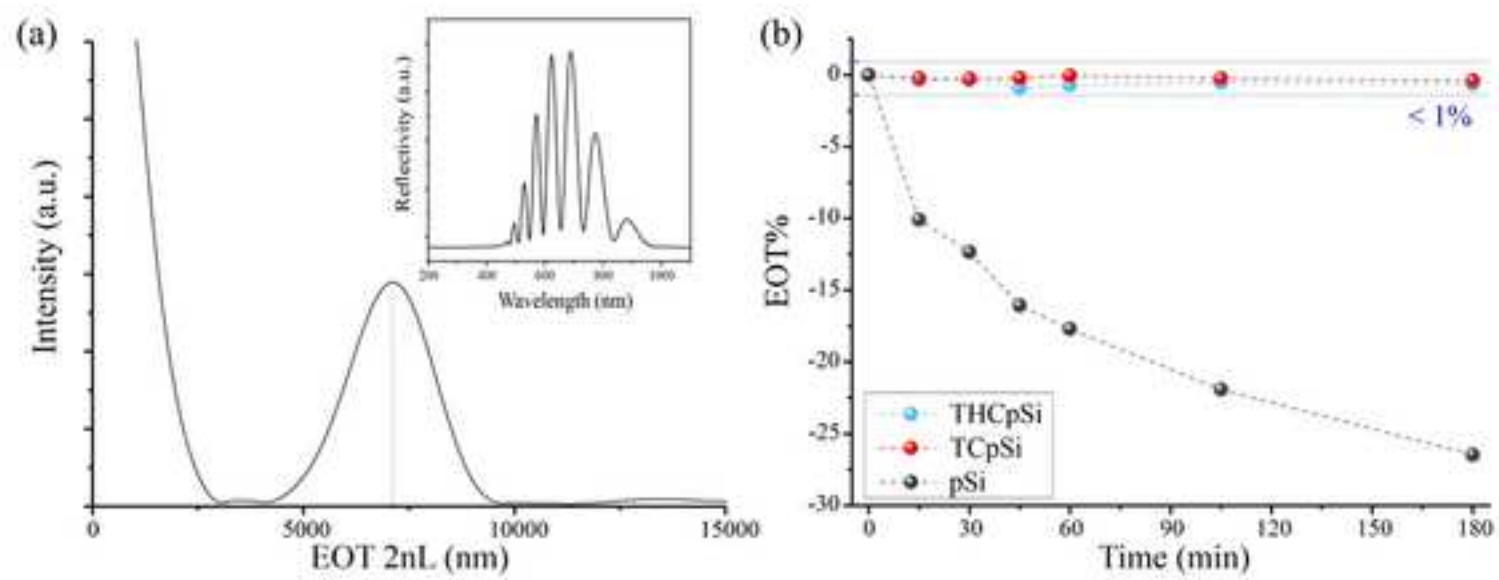


Figure 4

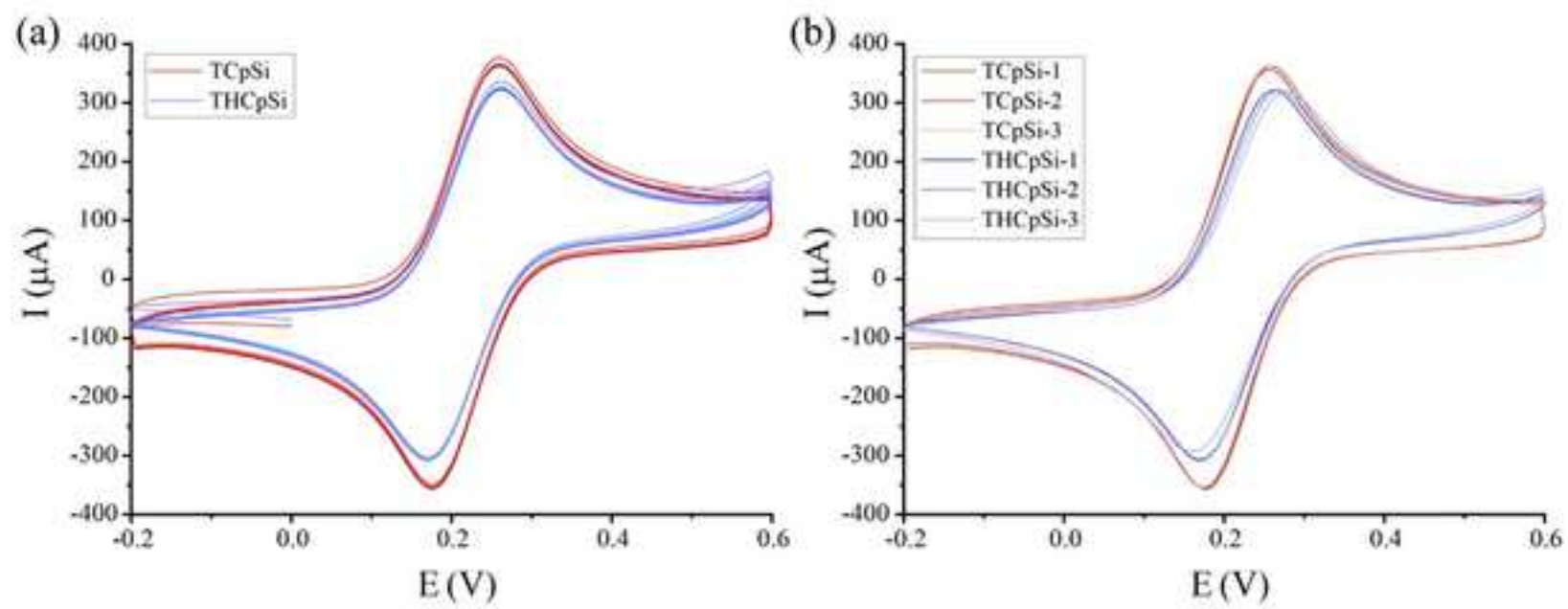


Figure 5

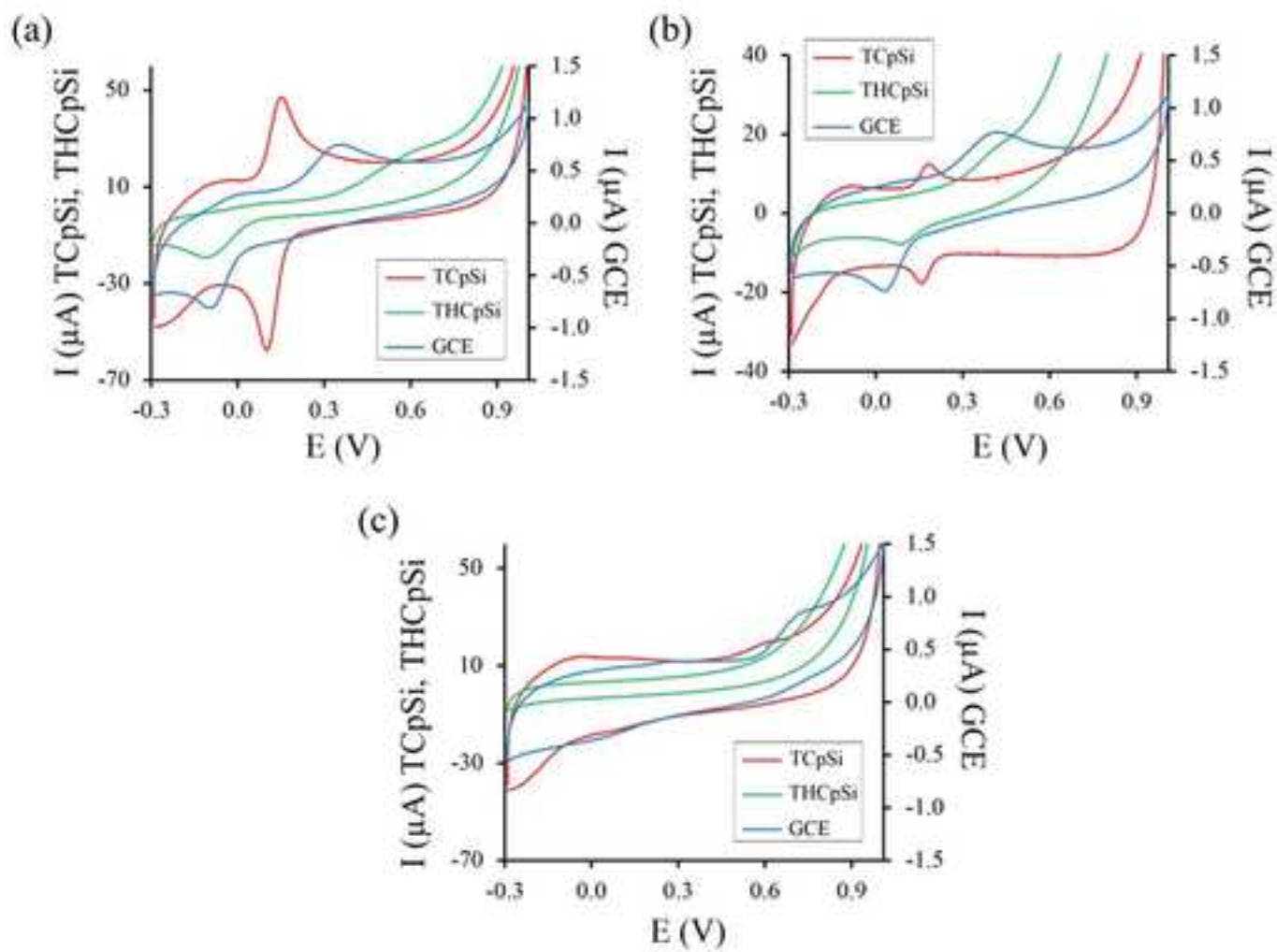


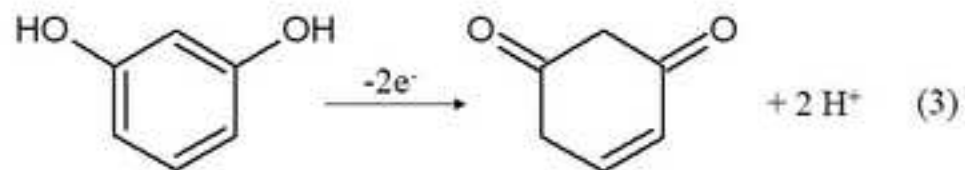
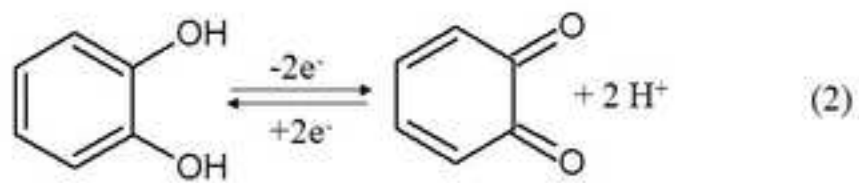
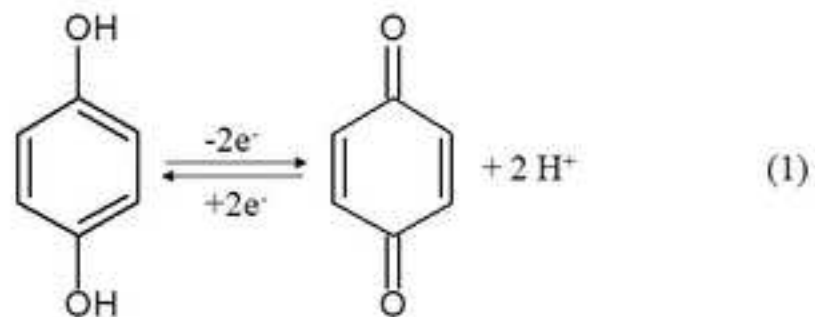
Figure 6

Figure 7

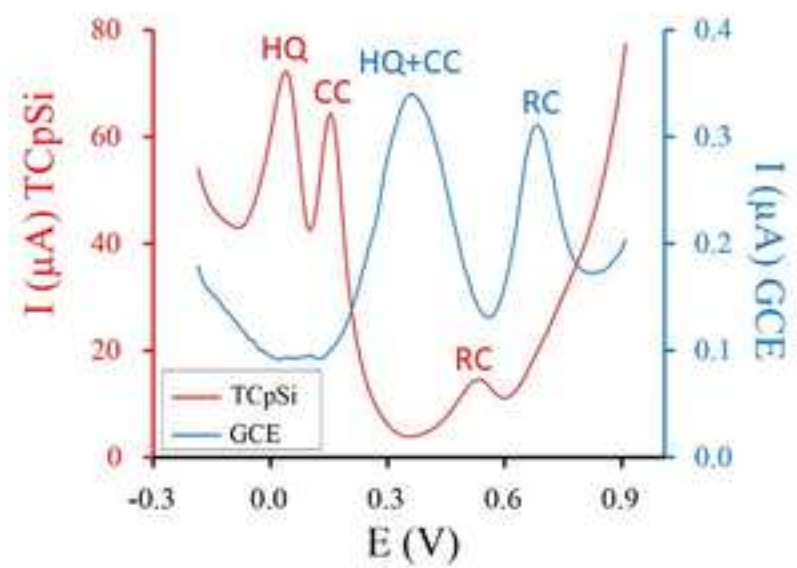


Figure 8

